

N69-34379  
CR-104066

**Gulf General Atomic**  
Incorporated

GA-9483

RADIATION EFFECTS IN SILICON SOLAR CELLS

QUARTERLY REPORT

by

J. A. Naber, B. C. Passenheim, and R. A. Berger

JULY 10, 1969

PREPARED FOR

CALIFORNIA INSTITUTE OF TECHNOLOGY  
Jet Propulsion Laboratory  
4800 Oak Grove Drive  
Pasadena, California 91103

CONTRACT 952387

This work was performed for the Jet Propulsion Laboratory, California Institute of Technology, as sponsored by the National Aeronautics and Space Administration under Contract NAS7-100.

CASE FILE  
COPY

# **Gulf General Atomic**

**Incorporated**

*P.O. Box 608, San Diego, California 92112*

GA-9483

## RADIATION EFFECTS IN SILICON SOLAR CELLS

### QUARTERLY REPORT

by

J. A. Naber, B. C. Passenheim, and R. A. Berger

Prepared for  
California Institute of Technology  
Jet Propulsion Laboratory  
4800 Oak Grove Drive  
Pasadena, California 91103

CONTRACT 952387

This work was performed for the Jet Propulsion Laboratory, California Institute of Technology, as sponsored by the National Aeronautics and Space Administration under Contract NAS7-100

Gulf General Atomic Project 6105

July 10, 1969

## FOREWORD

This report contains information prepared by Gulf General Atomic Incorporated under Jet Propulsion Laboratory subcontract. Its contents are not necessarily endorsed by the Jet Propulsion Laboratory, California Institute of Technology, or the National Aeronautics and Space Administration.

## ABSTRACT

The purpose of the contract is to ascertain the nature of the defect or defects responsible for the output degradation of silicon solar cells irradiated by space radiation. Present effort is concentrated on the effects of lithium on the production and annealing of damage in silicon.

Samples of high-purity silicon have been lithium diffused by the paint-on and lithium-tin bath techniques. Samples of various lithium content have been prepared, and the lithium content is being measured by room-temperature resistivity and neutron activation analysis techniques. Both neutron and electron irradiation programs have been initiated. Lifetime degradation rates at 273°K and 302°K have been measured as a function of neutron fluence. From isochronal and isothermal anneal data the annealing kinetics appear to be first order and are controlled by the diffusion rate of lithium in silicon. Results of the effect of the lithium concentration on the degradation and annealing of electron-irradiated lithium-diffused n-type silicon have been obtained. An electron spin resonance study of the irradiation production and anneal of the divacancy has been initiated.

## CONTENTS

1. INTRODUCTION . . . . .	1
2. PROGRESS . . . . .	1
2.1 Electron Irradiations . . . . .	1
2.2 Neutron Irradiations . . . . .	7
2.2.1 Isochronal Anneal . . . . .	16
2.2.2 Isothermal Anneals . . . . .	19
2.3 Activation Analysis . . . . .	24
2.4 Electron Spin Resonance (ESR) . . . . .	27
2.4.1 Experimental . . . . .	27
2.4.2 Measurements . . . . .	30
3. ANALYSIS AND CONCLUSIONS . . . . .	31
4. PLANS FOR THE NEXT REPORTING PERIOD . . . . .	32
5. NEW TECHNOLOGY . . . . .	32
REFERENCES . . . . .	33

## FIGURES

1. Electrical conductivity as a function of $1000/T$ for lithium-diffused 11 ohm-cm n-type silicon . . . . .	3
2. Inverse temperature dependence of lifetime of 11 ohm-cm silicon . . . . .	4
3. Inverse lifetime versus 30-MeV electron fluence for the 11 ohm-cm lithium-diffused n-type silicon sample . . . . .	5
4. Inverse lifetime versus fluence for the 0.4 ohm-cm lithium-diffused n-type silicon irradiated with 30-MeV electrons at room temperature . . . . .	8
5. Preirradiation and postirradiation conductivity versus $1000/T$ for sample a . . . . .	9
6. Preirradiation and postirradiation electrical conductivity versus $1000/T$ for sample b . . . . .	10
7. Apparatus for measuring lifetime and resistivity as a function of neutron fluence . . . . .	12
8. Preirradiation and postirradiation minority-carrier lifetime versus $1000/T$ for neutron-irradiated 3.7 ohm-cm sample a . . . . .	13
9. Preirradiation lifetime versus $1000/T$ for 3.7 ohm-cm neutron-irradiated sample a using steady-state photoconductivity technique . . . . .	14

CONTENTS (continued)

10. Preirradiation lifetime versus $1000/T$ for 3.7 ohm-cm neutron-irradiated sample b using steady-state photoconductivity technique . . . . .	15
11. Degradation of inverse lifetime as a function of fluence . . . . .	17
12. Unannealed fraction of defects versus isochronal anneal temperature for neutron-irradiated 3.7 ohm-cm lithium-diffused n-type silicon . . . . .	18
13. Sample a isochronal anneal analysis . . . . .	20
14. Isothermal anneal of sample a . . . . .	21
15. Inverse lifetime versus neutron fluence irradiated and measured at room temperature . . . . .	23
16. Unannealed fraction versus isochronal anneal temperature for neutron-irradiated 3.7 ohm-cm sample b . . . . .	25
17. Unannealed fraction of annealable defects for $411^{\circ}\text{K}$ isothermal anneal versus time . . . . .	26
18. ESR spectrometer for lithium-doped silicon studies . . . . .	29

## 1. INTRODUCTION

The overall purpose of this program is to ascertain the nature of the defect or defects responsible for the decrease in minority-carrier lifetime in silicon irradiated by space radiation. When the nature of the defects and their annealing mechanisms are known, it will be possible to determine parameters that will lead to the development of radiation-hardened devices (silicon solar cells).

The present effort is concentrated on the study of the effects of lithium on the production and annealing of damage in silicon. This work is being performed on lithium-diffused bulk silicon using electrical measurements, such as minority-carrier lifetime, electron spin resonance (ESR), electrical conductivity, and Hall effect. The temperature range from 77.5°K to 400°K is under investigation. The damage is introduced by 30-MeV electrons and fission neutrons.

## 2. PROGRESS

### 2.1 ELECTRON IRRADIATIONS

To date, two samples of lithium-diffused silicon have been subjected to 30-MeV electron irradiations.

The first sample was made from  $10^4$  ohm-cm n-type float-zone-grown silicon by the lithium-tin bath technique.<sup>(1)</sup> Its initial room-temperature resistivity was 11 ohm-cm. This corresponds to an estimated lithium content of  $n_0 = 4.5 \times 10^{14} \text{ cm}^{-3}$ . Gold preforms were attached to a 1.6 x 1.6 x 9.1 mm sample by heating it to 450°C for 7 min. Four leads were then soldered to the gold dots and the sample was mounted in a cryostat.<sup>(2)</sup> The preirradiation temperature dependence of the electrical conductivity is shown

in Fig. 1. Figure 2 shows the preirradiation temperature dependence of the low-injection-level excess carrier lifetime. The conductivity decreases with increasing temperature because the temperature dependence of the lattice scattering.<sup>(3)</sup> The preirradiation excess carrier lifetime decreases with temperature slightly too rapidly to be entirely due to the temperature dependence of the capture cross section for an attractive singly charged center.<sup>(4)</sup> However, it is clearly too severe to be due to a neutral center. The temperature dependence of lifetime for an attractive center is indicated on Fig. 1 for comparison. The Fermi level for this sample ranges from 0.1 to 0.4 eV from the band edge.

In the minority-carrier lifetime measurements, excess carriers were injected into the samples by two techniques, with a xenon strobe light and with a 600-keV flash X-ray. The same lifetime was measured by both these techniques.

The sample was then taken to the Gulf General Atomic linear accelerator (Linac) and the minority-carrier lifetime was measured as a function of fluence at room temperature. The sample was damaged by 4.5  $\mu$ sec pulses with fluences of  $2.5 \times 10^{11}$  e/cm<sup>2</sup> per pulse. Low injection levels for lifetime measurements were accomplished by shortening the Linac pulse to 0.4  $\mu$ sec, defocusing the beam, and reducing the beam intensity. The initial room-temperature minority-carrier lifetime of 55  $\mu$ sec was reduced to 1  $\mu$ sec by a fluence of  $\phi = 2.2 \times 10^{13}$  (e/cm<sup>2</sup>). As shown in Fig. 3, the initial degradation constant K (defined by  $1/\tau = 1/\tau_0 + K\phi$ ) is about  $7 \times 10^{-8}$  (cm<sup>2</sup>/e-sec). The degradation constant appears to decrease to about  $3 \times 10^{-8}$  (cm<sup>2</sup>/e-sec) at fluences greater than  $1 \times 10^{13}$  e/cm<sup>2</sup>. There are two possible explanations for this. One is that the lithium in this sample was depleted at such fluences. The other reason is that room-temperature annealing may have occurred during the irradiation. These K factors are lower than  $1.1 \times 10^{-7}$  (cm<sup>2</sup>/e-sec), previously measured for silicon doped to concentrations of  $10^{16}$  to  $10^{17}$  cm<sup>-3</sup>, and are closer to  $K \approx 6 \times 10^{-8}$  (cm<sup>2</sup>/e-sec) for silicon without lithium. The sample was then isothermally annealed at

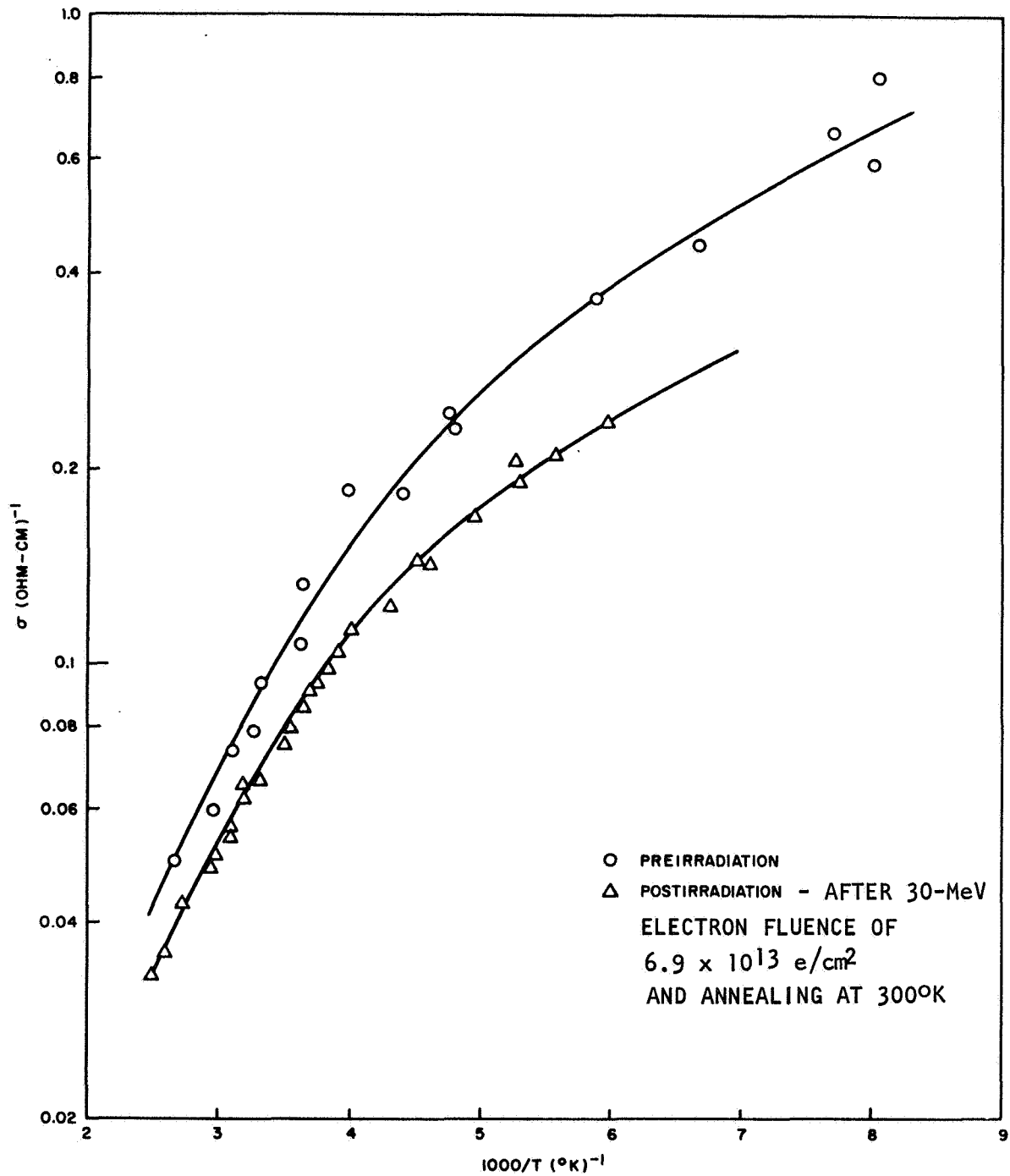


Fig. 1--Electrical conductivity as a function of 1000/T for lithium-diffused 11 ohm-cm n-type silicon

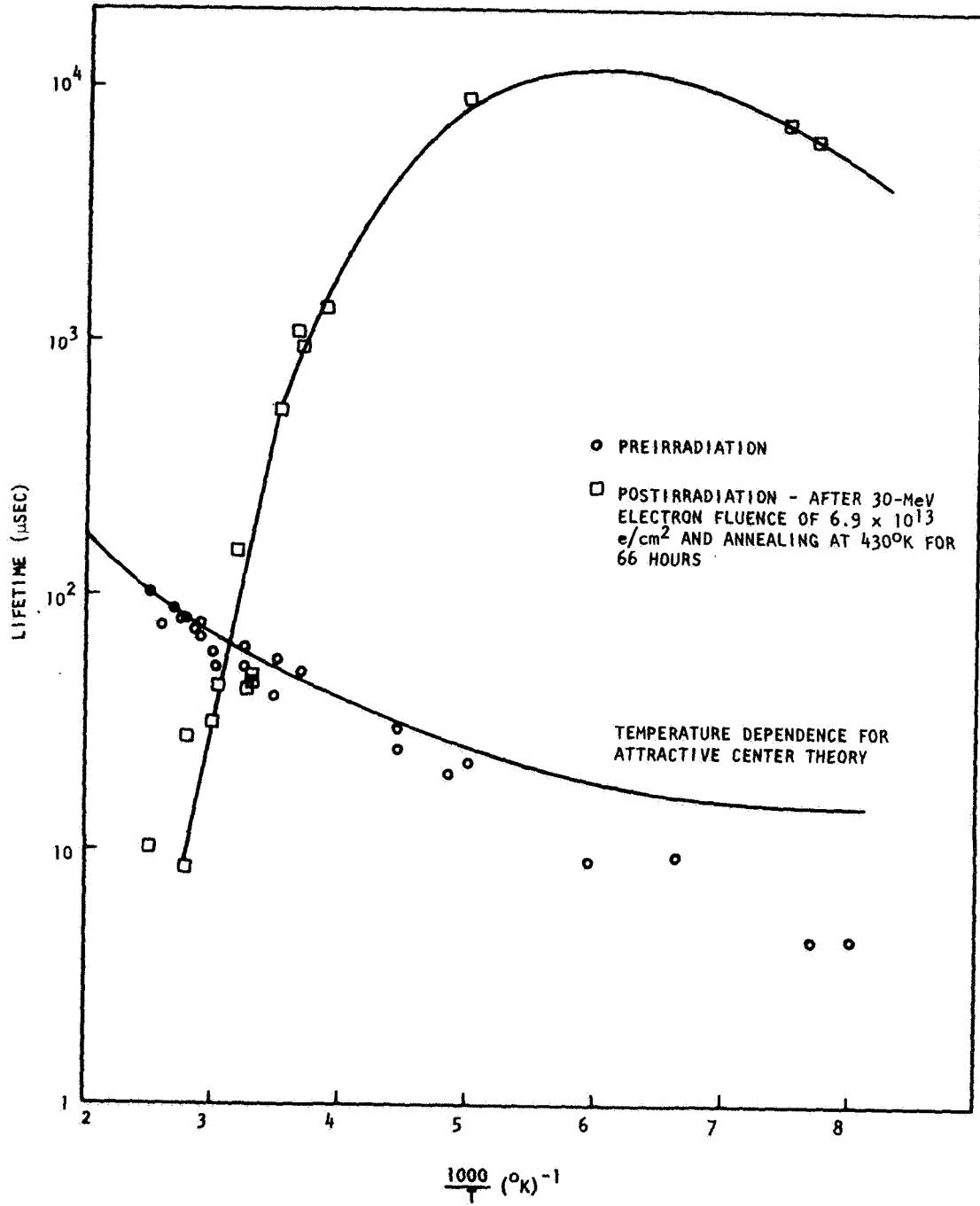


Fig. 2--Inverse temperature dependence of lifetime of 11 ohm-cm silicon

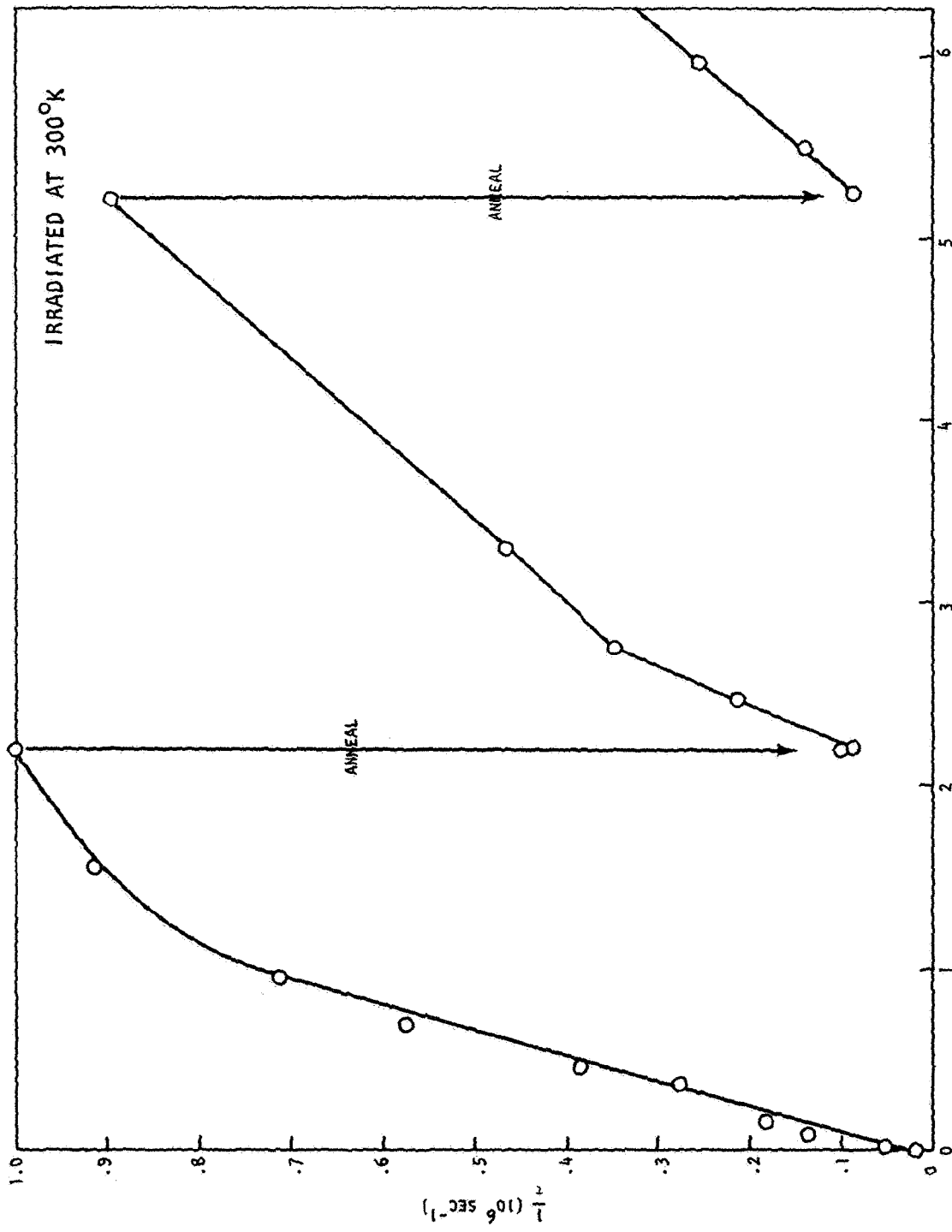


Fig. 3--Inverse lifetime versus 30-MeV electron fluence for the 11 ohm-cm lithium-diffused n-type silicon sample

355°K for about 1 hour and at 380°K for about 40 min. After this anneal, the minority-carrier lifetime had returned to 10 μsec, indicating nearly 90-percent anneal in the number of recombination centers. The number of recombination centers can be related to the carrier lifetime by

$$\tau = \frac{1}{Nv\sigma}$$

where N is the density of recombination centers, v is the thermal velocity of the carriers and σ is the capture cross section of the recombination center for the carrier.

After the anneal, the minority-carrier lifetime was again reduced to 1.1 μsec by an additional fluence of  $\varphi = 3 \times 10^{13}$  e/cm<sup>2</sup> and annealed again at ~ 420°K. After the second anneal, a trapping center was clearly apparent by an excess conductivity decay time which increased with decreasing temperature. The sample was irradiated to a total fluence of  $6.9 \times 10^{13}$  e/cm<sup>2</sup>. At this fluence level, the trapping at room temperature was so great that the recombination lifetime could not be determined. This trapping center could not be removed by annealing at 430°K for 66 hours. This annealing did not indicate any alteration of the properties of the trapping center or annealing of the radiation-introduced recombination centers.

The appearance of a trapping center after irradiation with 30-MeV electrons was previously noted<sup>(5)</sup> for the high-purity n-type silicon, which was our starting material prior to lithium diffusion.

The postirradiation lifetime and conductivity as a function of temperature were measured and are presented in Figs. 1 and 2.

The second sample subjected to 30-MeV electron irradiation was made from the same  $10^4$  ohm-cm n-type silicon by the lithium-oil paint-on technique. Its initial room-temperature resistivity was 0.4 ohm-cm ( $n_0 \approx 1.5 \times 10^{16}$  cm<sup>-3</sup>). The minority-carrier-lifetime sample was measured as

previously described. The initial room-temperature lifetime was 4.5  $\mu$ sec. This sample was also irradiated at room temperature, and Fig. 4 shows the lifetime degradation and anneal as a function of fluence. The degradation constant shows considerable variation, which we cannot presently explain; it is about  $1.8 \pm 0.3 \times 10^{-7}$   $\text{cm}^2/\text{e-sec}$ . The lifetime was degraded to less than 1  $\mu$ sec three times and completely recovered with 30 min anneals at 370 $^\circ$ K. After the sample was degraded and annealed three times, it was exposed to a total fluence of  $4 \times 10^{14}$  ( $\text{e}/\text{cm}^2$ ). After this fluence the sample was isothermally annealed for 30 min at 370 $^\circ$ K and 420 $^\circ$ K. The room-temperature lifetime recovered from less than 0.5  $\mu$ sec to about 1.6  $\mu$ sec, which implies approximately 80 percent of the radiation-induced recombination centers were annealed. No trapping was observed at room temperature.

In summary, the degradation constant for heavily lithium-diffused silicon is greater than for lightly diffused or nondiffused silicon. Annealing is observed at temperatures below 400 $^\circ$ K, but the ability to anneal appears to be inhibited as the fluence is increased. The greater the initial lithium content, the greater the fluence required to substantially inhibit recovery. The degradation constant decreases as the total fluence increases. These observations appear consistent with the idea that lithium is depleted during the production and annealing of radiation-produced recombination centers.

## 2.2 NEUTRON IRRADIATIONS

Two 3.7 ohm-cm samples were made from  $10^4$  ohm-cm n-type float-zone-grown silicon by the lithium-tin bath technique. They were similar in every respect but their  $l/A$  ratio ( $l$  = distance between voltage probes,  $A$  = cross-sectional area); sample a had  $l/A = 8.37 \text{ cm}^{-1}$ , and sample b,  $l/A = 7.43 \text{ cm}^{-1}$ . Figures 5 and 6 show the preirradiation and post-irradiation conductivity versus temperature for samples a and b, respectively.

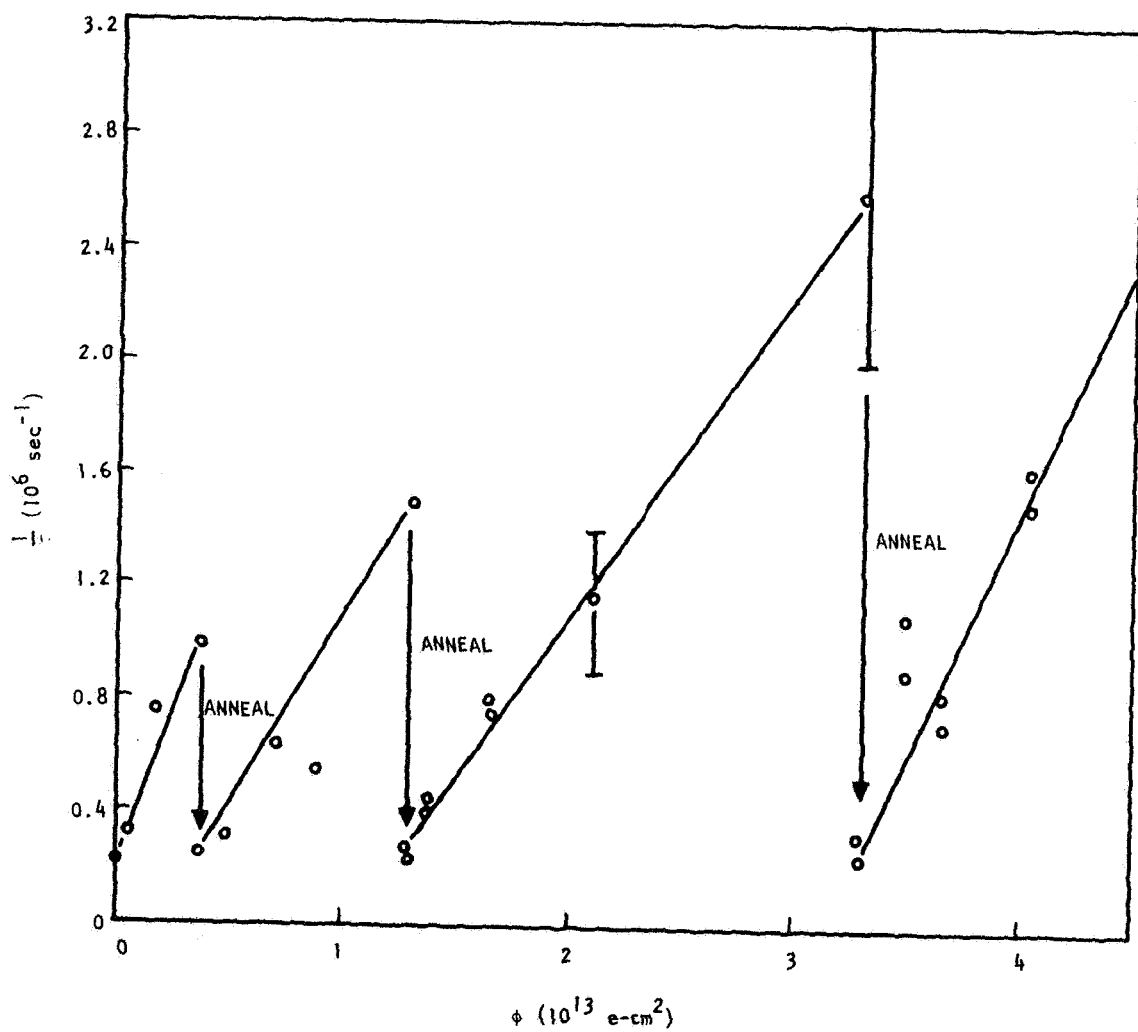


Fig. 4--Inverse lifetime versus fluence for the 0.4 ohm-cm lithium-diffused n-type silicon irradiated with 30-MeV electrons at room temperature

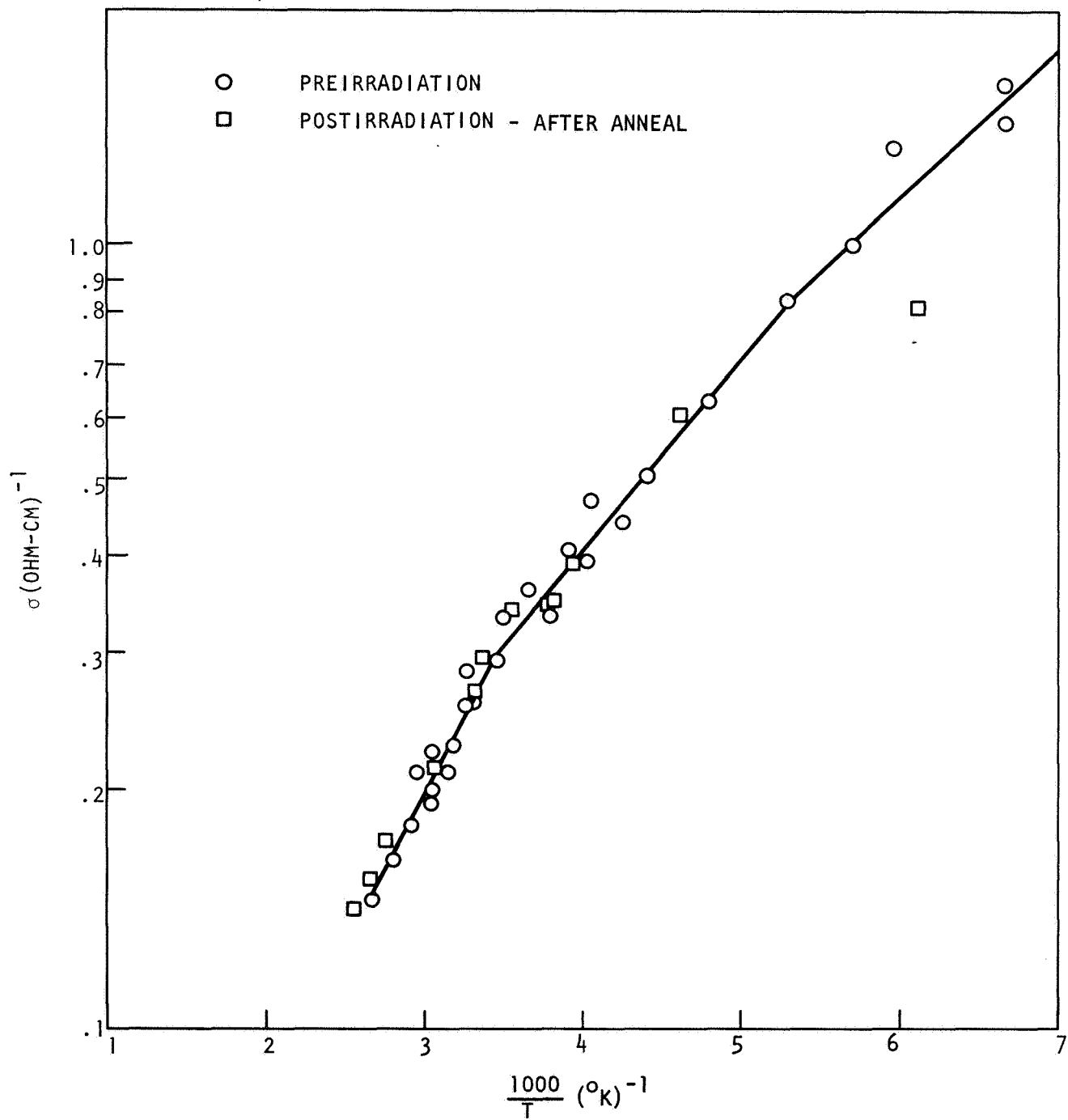


Fig. 5--Preirradiation and postirradiation conductivity versus  $1000/T$  for sample a

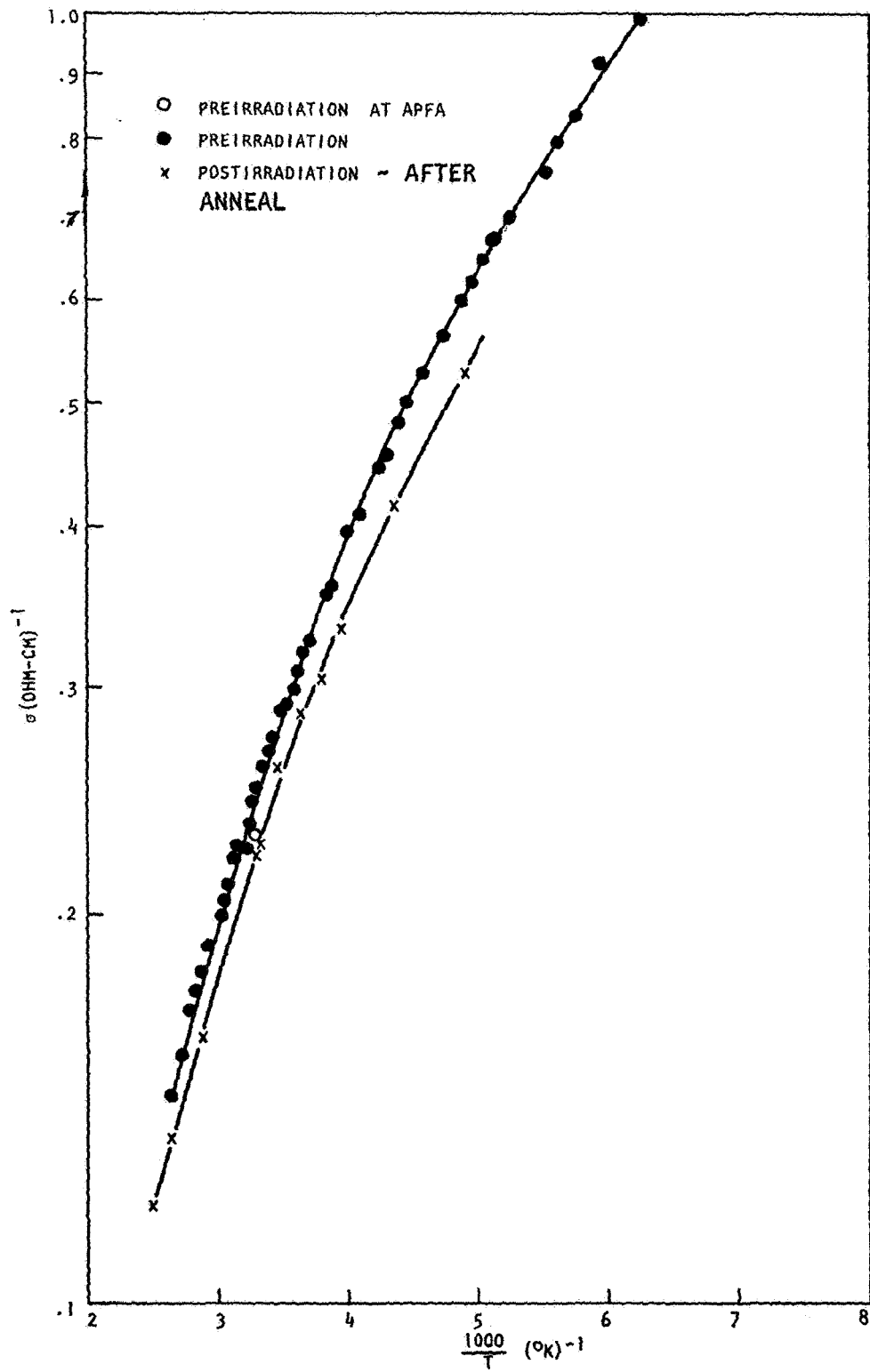


Fig. 6--Preirradiation and postirradiation electrical conductivity versus  $1000/T$  for sample b

These samples were mounted in a vacuum chamber used previously to study solar cells. This apparatus is schematically illustrated in Fig. 7. Minority carriers are injected with a tungsten filament light source, which is passed through a lens system, water, GaAs, and Si filters, and is chopped by a toothed wheel at  $10^3$  Hz. The change in conductivity is  $\Delta\sigma = g\tau e(\mu_n + \mu_p)$ , where  $g$  is the generation rate of the light source, and the direct current conductivity is  $\sigma_0 = n_0 e\mu_n$ . This is known as the steady-state photoconductivity technique. Thus, holding the sample current constant, one finds that

$$\frac{\Delta V}{V} = \frac{\Delta\sigma}{\sigma_0} = \frac{\Delta n}{n_0} = \frac{g\tau}{n_0} \left( \frac{\mu_n + \mu_p}{\mu_n} \right) .$$

The signal observed was dc voltage ( $V$ ) modulated by a  $10^3$ -Hz chopped signal of amplitude  $\Delta V = 10^{-3}$  V. From the above equation, it is clear that

$$\tau = \frac{n_0}{g} \left( \frac{\mu_n}{\mu_n + \mu_p} \right) \frac{\Delta V}{V} = A \frac{\Delta V}{V} .$$

The constant  $A$  was empirically determined to be  $A_a = 2.95 \times 10^{-2}$  sec for sample a and  $A_b = 2.26 \times 10^{-2}$  sec for sample b at  $300^\circ\text{K}$ . Figure 8 shows the preirradiation and postirradiation minority-carrier lifetime as a function of temperature for sample a. These data are obtained from photoconductivity decay. Figures 9 and 10 show the preirradiation temperature dependence of  $\Delta V/V$  for samples a and b. These data can be used to determine  $\tau$  as a function of temperature once the temperature dependence of the mobilities is known.

These samples were subjected to neutron irradiations at Gulf General Atomic's accelerator pulsed fast assembly (APFA) facility. APFA was run in the continuous (steady-state) mode at 5 watts. This setting corresponds

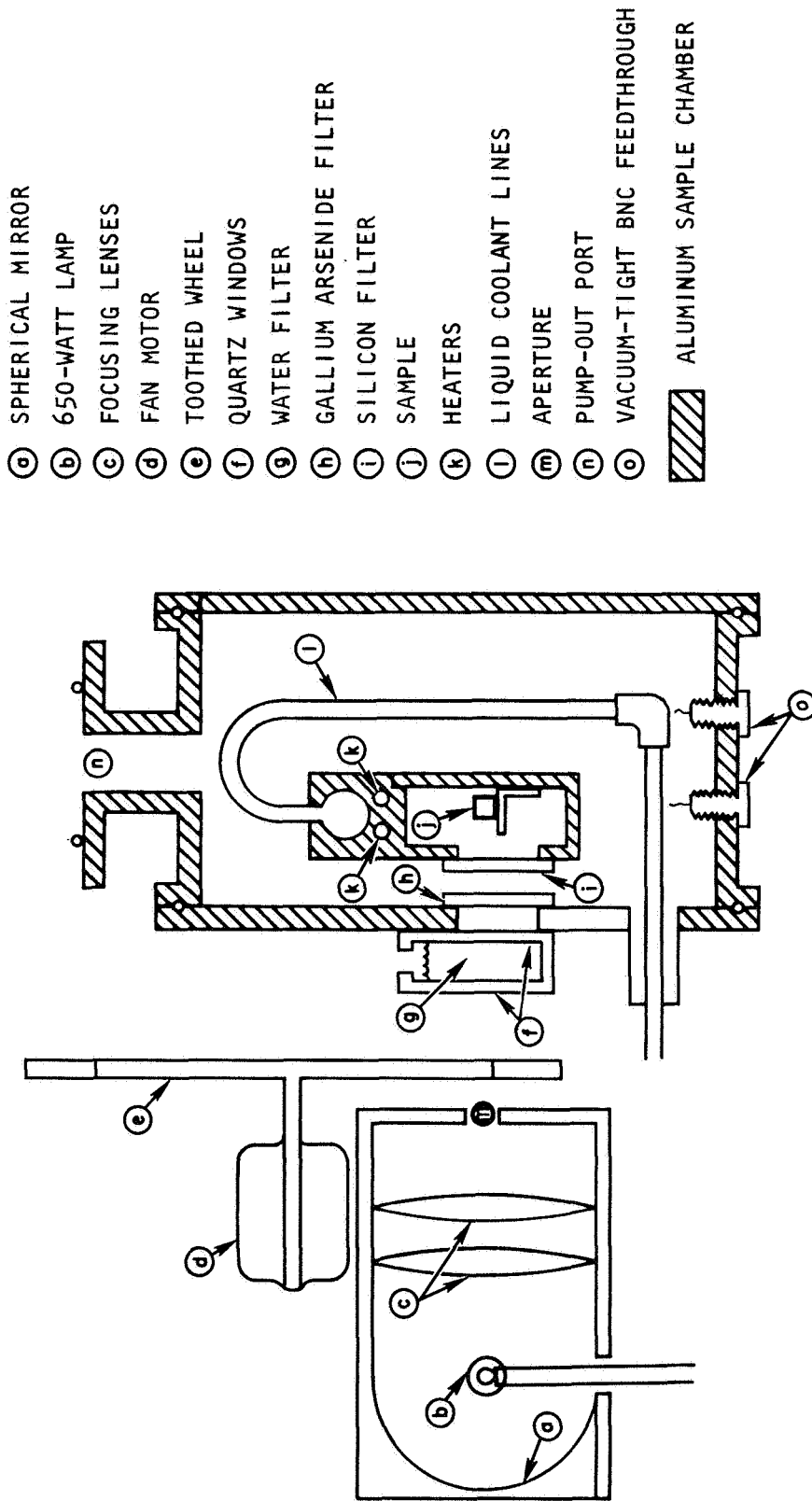


Fig. 7--Apparatus for measuring lifetime and resistivity as a function of neutron fluence  
(not to scale)

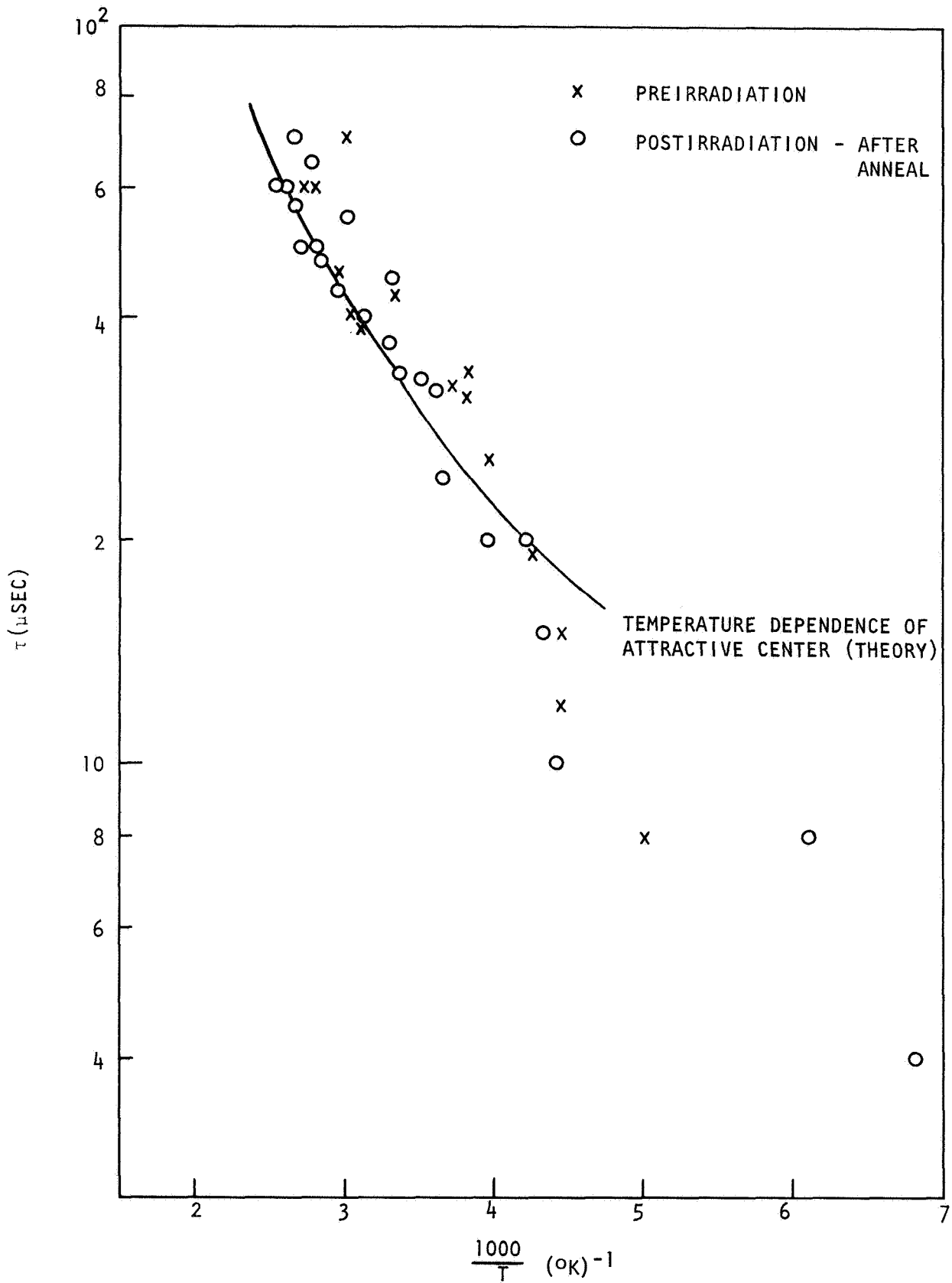


Fig. 8--Preirradiation and postirradiation minority-carrier lifetime versus  $1000/T$  for neutron-irradiated 3.7 ohm-cm sample a. Data taken using photoconductivity decay technique

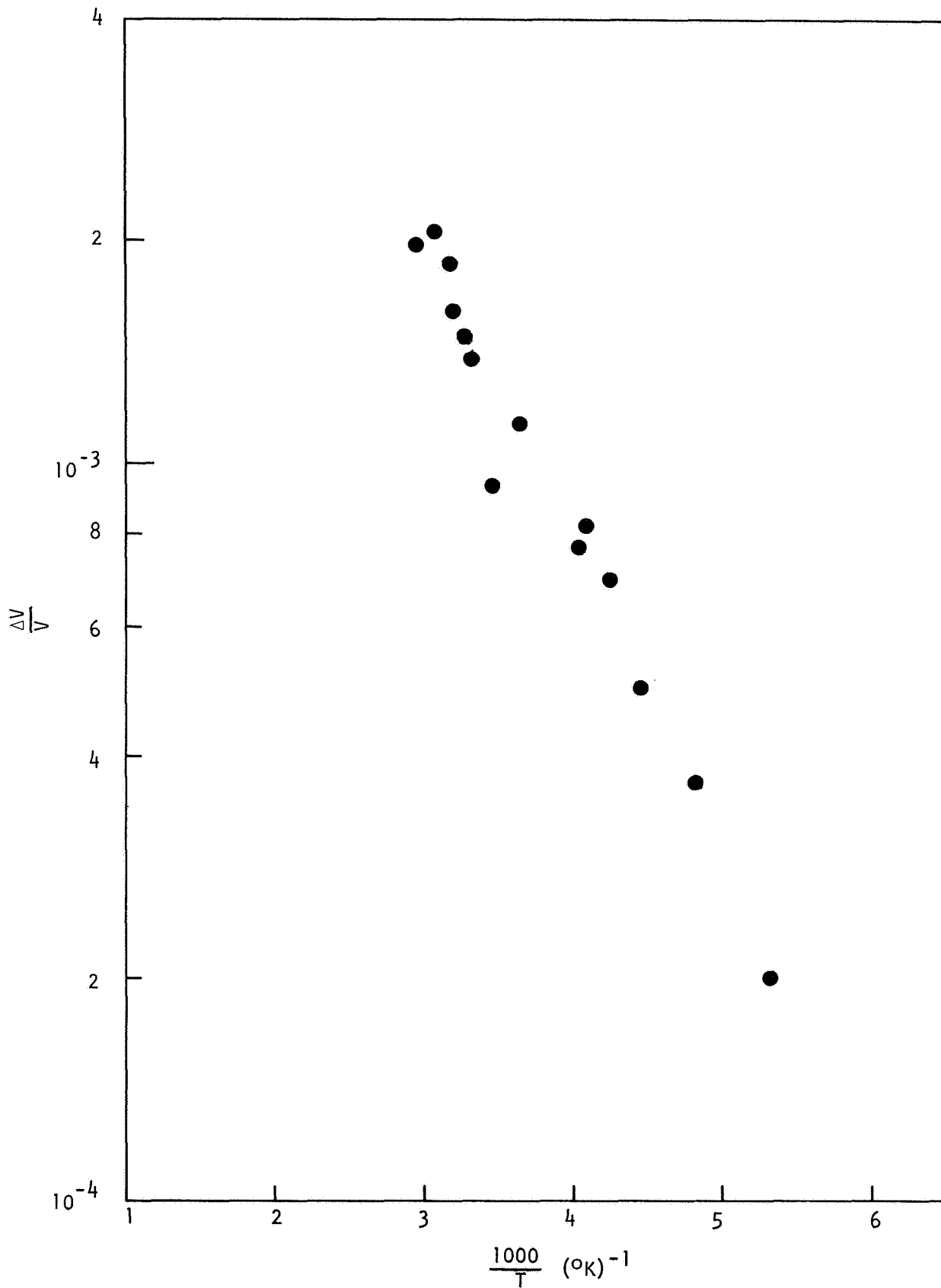


Fig. 9--Preirradiation lifetime versus  $1000/T$  for 3.7 ohm-cm neutron-irradiated sample a using steady-state photo-conductivity technique

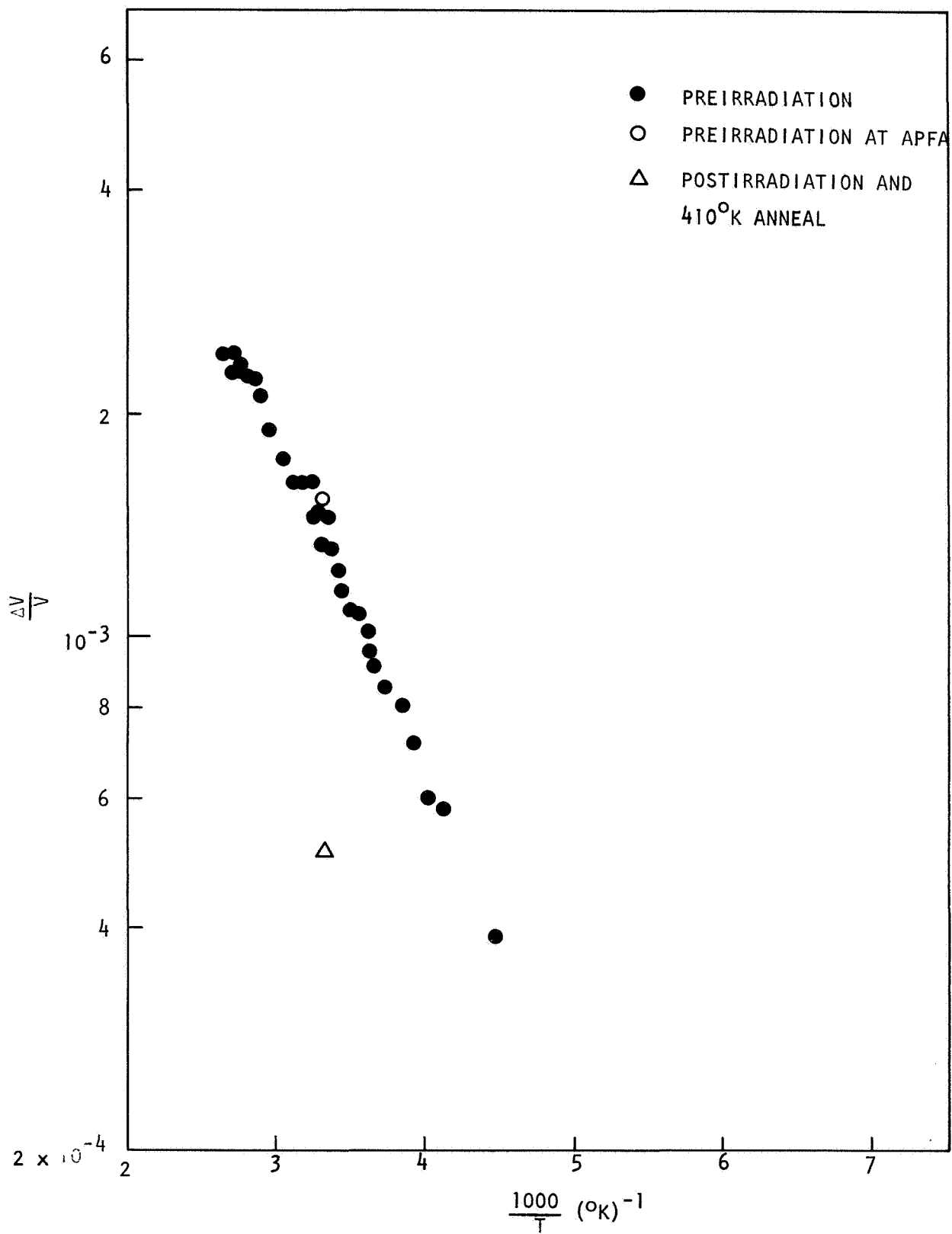


Fig. 10--Preirradiation lifetime versus  $1000/T$  for 3.7 ohm-cm neutron-irradiated sample b using steady-state photoconductivity technique

to  $7.5 \times 10^8$  (n/cm<sup>2</sup>-W-min) (E > 10 keV). Fluences were verified with sulfur pellet dosimeters. Sample a was irradiated at 273°K; sample b at 302°K. Sample a had an initial 273°K lifetime of 30 μsec; this was reduced to about 5 μsec by a fluence of  $2.25 \times 10^{10}$  (n/cm<sup>2</sup>). The sample was isochronally annealed for 5-min periods at temperatures up to 411°K, degraded again, isothermally annealed at 393°K, degraded a third time, and then isothermally annealed at 411°K. Figure 11 shows  $1/\tau$  versus fluence  $\Phi$ . Better than 90 percent of the damage introduced by the first irradiation was annealed. Apparently all the damage introduced by the next two irradiations was annealed. The degradation constant was found to be  $(6.4 \pm 0.4) \times 10^{-6}$  (cm<sup>2</sup>/n-sec) and independent of the total fluence, up to  $\Phi = 6.75 \times 10^{10}$  n/cm<sup>2</sup>. The degradation constant is also very nearly the same as that observed in nonlithium-diffused silicon,<sup>(6)</sup> as might be expected.

### 2.2.1 Isochronal Anneal

Isochronal anneal data were taken by rapidly heating the sample to an elevated temperature, holding it at that temperature for 5 min, and rapidly cooling it to 273°K, where the lifetime (as evidenced by  $\Delta V/V$ ) was remeasured.

Figure 12 shows the unannealed fraction of the total and annealable defects as a function of anneal temperature. The unannealed fraction of annealable defects is given by

$$f_T = \frac{(1/\tau_T) - (1/\tau_f)}{(1/\tau_0) - (1/\tau_f)} = \frac{(V/\Delta V)_T - (V/\Delta V)_f}{(V/\Delta V)_0 - (V/\Delta V)_f},$$

where  $\tau_T$  = observed lifetime at 273°K after 5-min anneal at temperature T,

$\tau_0$  = lifetime at 273°K immediately after irradiation,

$\tau_f$  = observed lifetime after annealing has ceased.

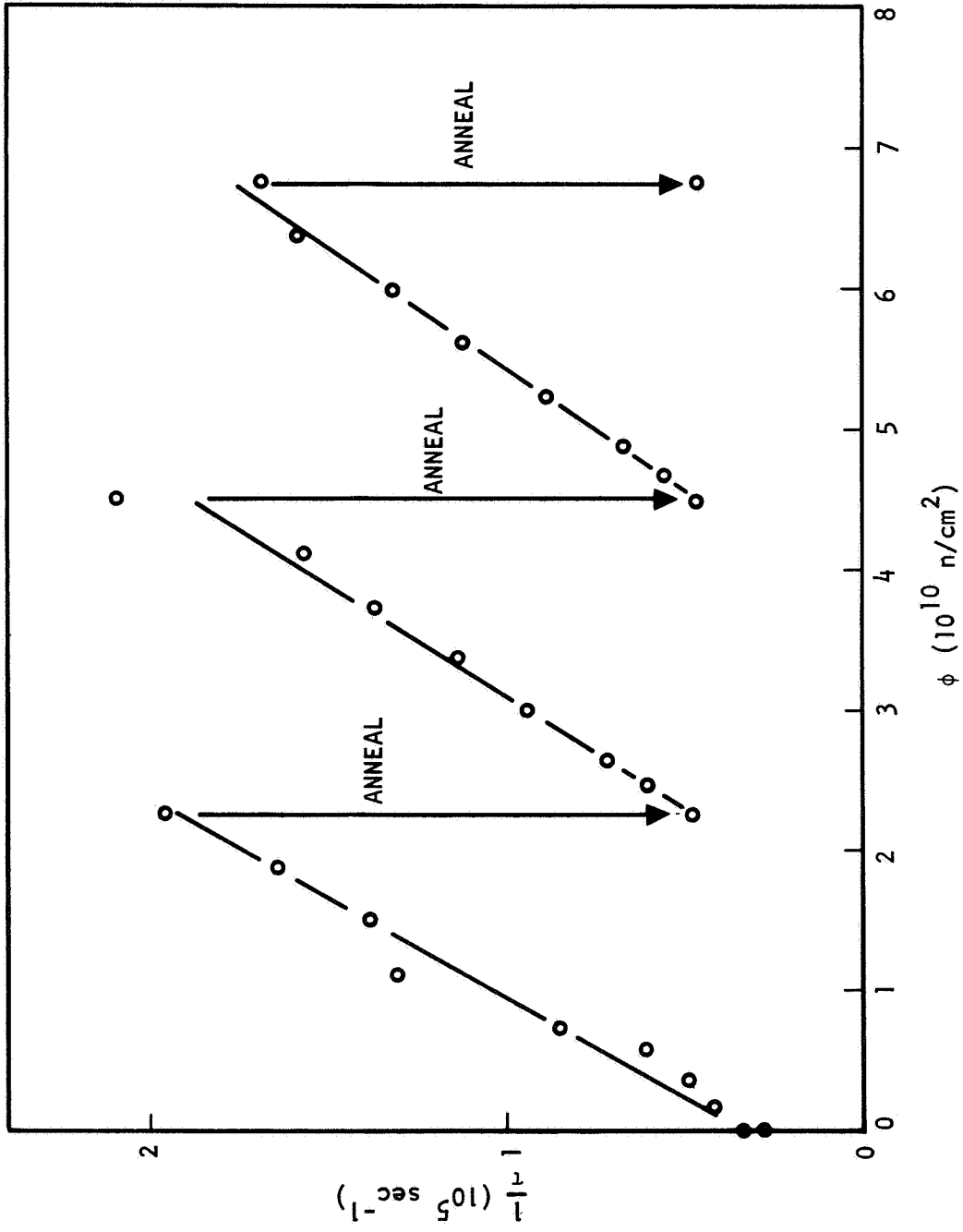


Fig. 11--Degradation of inverse lifetime as a function of fluence

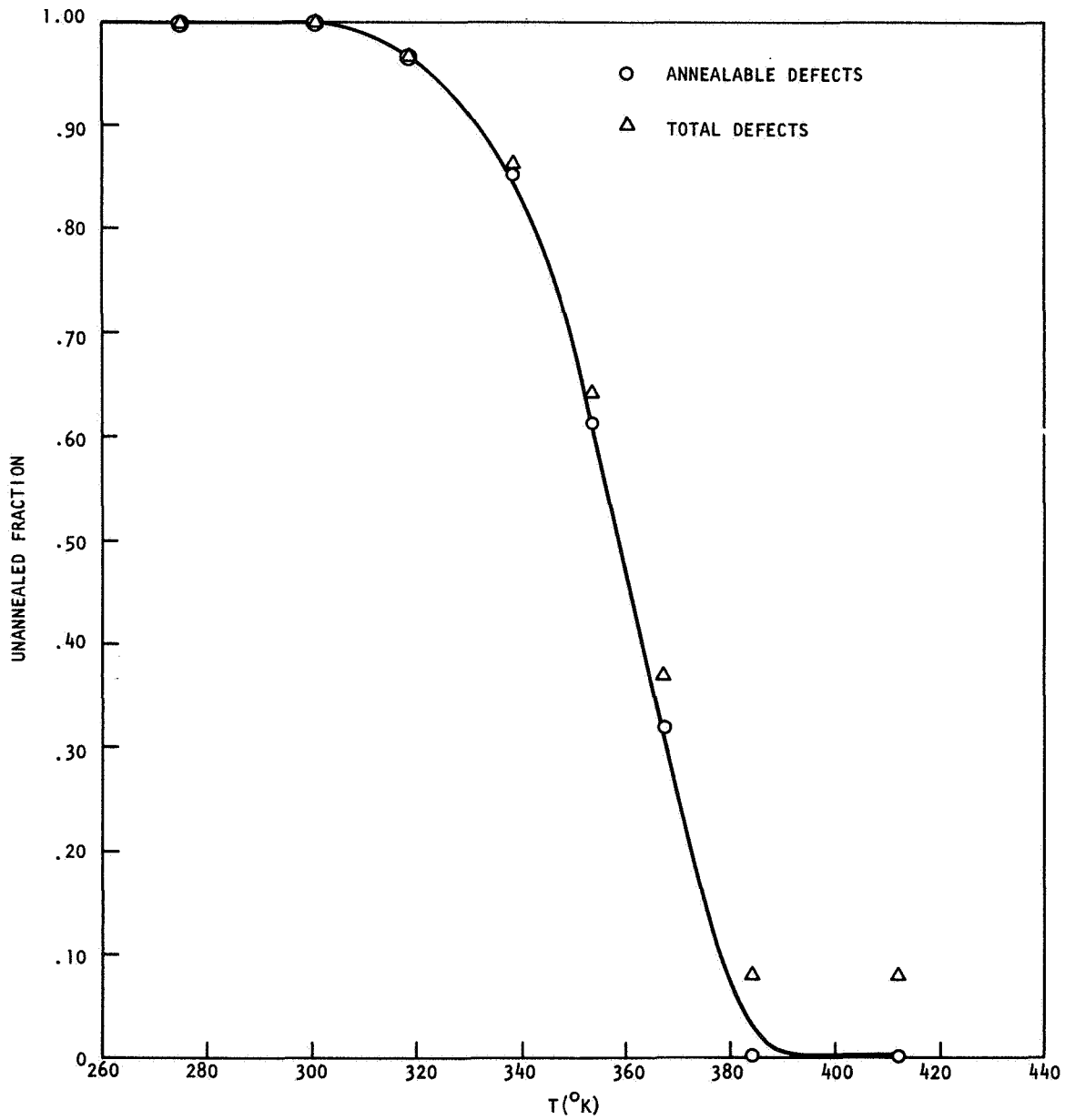


Fig. 12--Unannealed fraction of defects versus isochronal anneal temperature for neutron-irradiated 3.7 ohm-cm lithium-diffused n-type silicon

Assuming first-order kinetics, the number of recombination centers at time  $t$  is given by  $N(t) = N_0 e^{-Rt}$ , where the rate constant  $R$  is

$$R = \nu_0 e^{-E/kT} ,$$

where  $\nu_0$  = atomic frequency factor,

$E$  = activation energy.

Figure 13 is a semilogarithmic plot of  $\ln (N/N_T)$  versus  $100/T$ , where  $N$  is the number of recombination centers prior to a 5-min anneal at temperature  $T$  and  $N_T$  is the number present after the anneal. The values of  $N$  and  $N_T$  were always measured at the irradiation temperature of  $273^\circ\text{K}$  or  $302^\circ\text{K}$  before and after the anneal. From the data of Fig. 13, the activation energy was found to be  $E = 0.69 \pm 0.02$  eV. The atomic frequency factor was  $\nu_0 = (1.5 \pm 0.1) \times 10^7$  ( $\text{sec}^{-1}$ ).

### 2.2.2 Isothermal Anneals

The sample was isothermally annealed at  $393^\circ\text{K}$  and  $411^\circ\text{K}$ . Again, the sample was rapidly heated ( $t < 60$  sec) to the anneal temperature and held there until changes in the minority-carrier lifetime (exhibited as  $\Delta V/V$ ) were observed to cease. Figure 14 shows the unannealed fraction,

$$f(t) = \frac{(V/\Delta V)_t - (V/\Delta V)_\infty}{(V/\Delta V)_0 - (V/\Delta V)_\infty} ,$$

of annealable defects as a function of time  $t$ .

Assuming first-order kinetics  $N(t) = N_0 e^{-Rt}$  and  $R = \nu_0 e^{-E/kT}$ , one may determine the activation energy and the atomic frequency factor from any two isothermal anneals. The linearity of Fig. 14 is evidence that the annealing kinetics are, indeed, first order.

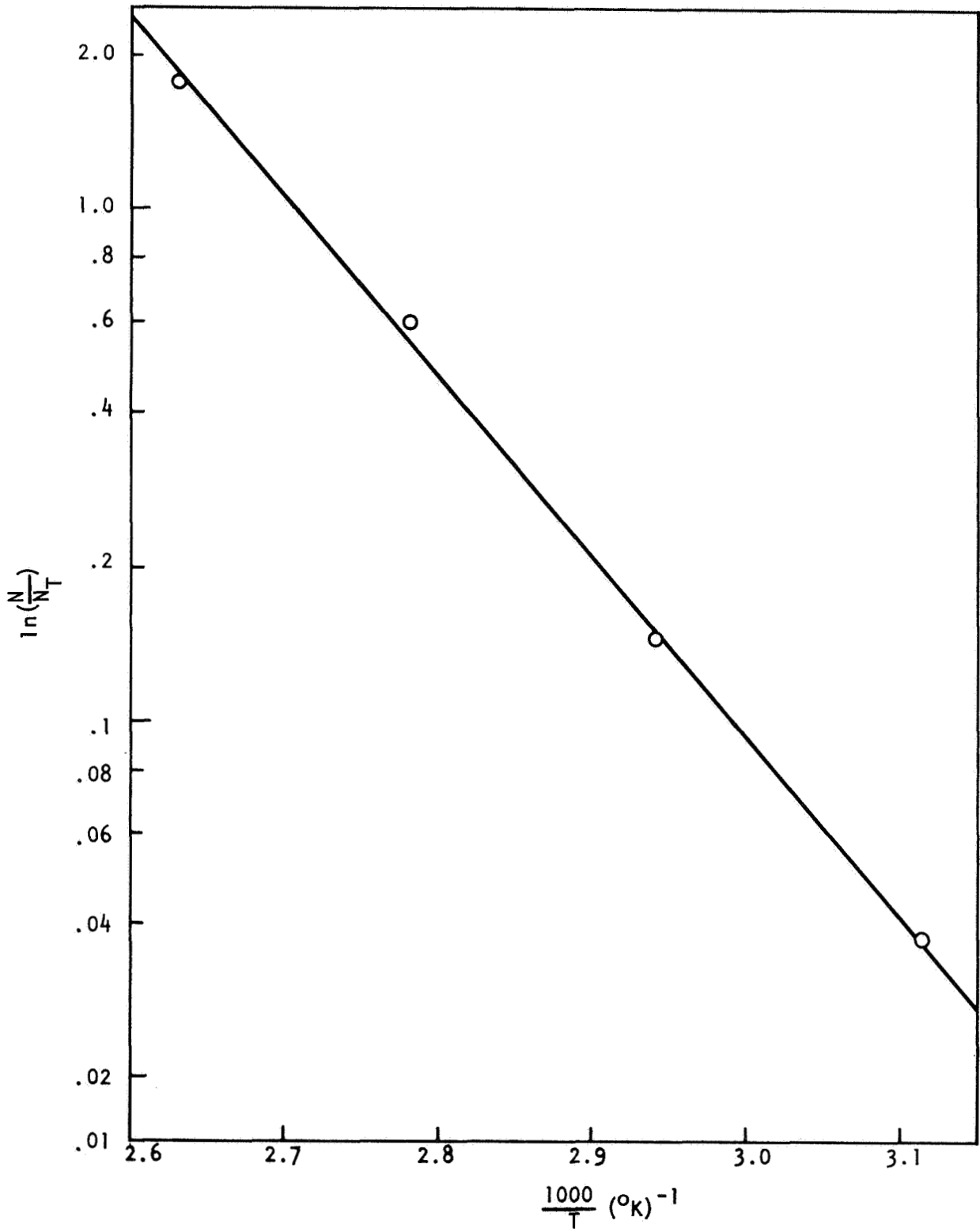


Fig. 13--Sample a isochronal anneal analysis

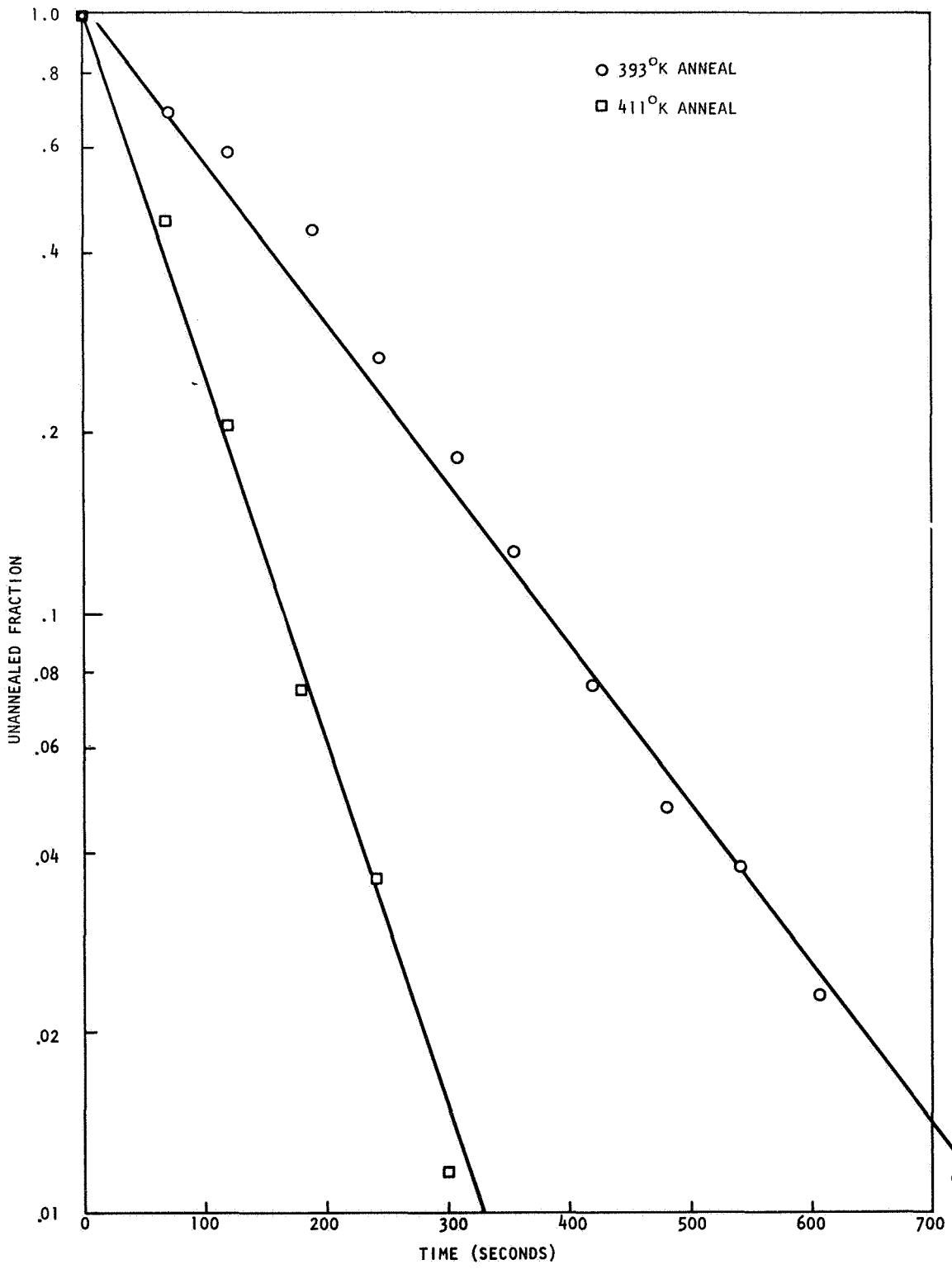


Fig. 14--Isothermal anneal of sample a

For sample a, isothermal anneal data indicate that  $E \approx 0.67 \pm 0.2$  eV and  $\nu_0 = (0.5 \pm 0.1) \times 10^7 \text{ sec}^{-1}$ . These results are in agreement with the isochronal results and yield an activation energy close to that of lithium diffusion in the silicon lattice.<sup>(7)</sup> The atomic frequency factor is quite low compared to  $\nu = 10^{11} \text{ sec}^{-1}$ , which was observed for electron-irradiated lithium-diffused silicon.<sup>(8)</sup>

Figure 8 shows both the preirradiation and postirradiation minority-carrier lifetime of sample a. These data were taken using the photoconductivity decay technique. The light was filtered with water, GaAs, and silicon before it impinged on the sample. Figure 5 shows the preirradiation and postirradiation conductivity of the sample. It is clear that the sample completely recovered after a total fluence of  $6.8 \times 10^{10} \text{ (n/cm}^2\text{)}$  with a 10-min anneal at  $411^\circ\text{K}$ .

In an effort to detect lithium depletion, sample b was subjected to higher-fluence neutron irradiations. The sample was irradiated at room temperature ( $T = 302^\circ\text{K}$ ) to determine whether the degradation constant was a strong function of temperature. The initial room-temperature lifetime of  $\sim 30 \mu\text{sec}$  was degraded to about  $2 \mu\text{sec}$  by a fluence of  $4.5 \times 10^{10} \text{ (n/cm}^2\text{)}$ . The degradation constant at  $302^\circ\text{K}$  was found to be  $K = (6.4 \pm 0.4) \times 10^{-6} \text{ cm}^2/\text{n-sec}$ , the same degradation rate found for sample a at  $273^\circ\text{K}$  and very nearly the same as for phosphorus-doped float-zone silicon ( $K \approx 5.8 \times 10^{-6}$ ) of equivalent resistivity.<sup>(6)</sup> Figure 15 shows the inverse lifetime versus fluence. Four irradiations are represented, three to fluences of  $4.5 \times 10^{10} \text{ n/cm}^2$  and one to  $\phi \approx 1.3 \times 10^{11} \text{ n/cm}^2$ . Between the first and second irradiations, the sample was isochronally annealed at temperatures up to  $440^\circ\text{K}$ . Between the first and second irradiations, about 90 percent of the radiation-induced damage was annealed. Half of the remaining 10 percent may be due to a reverse anneal which was apparent at  $T > 420^\circ\text{K}$ . After the other runs, the sample was isothermally annealed at  $T = 411^\circ\text{K}$ . The degradation constant was  $(6.4 \pm 0.4) \times 10^{-6} \text{ cm}^2/\text{n-sec}$  for all runs except the final and largest one, in which, at  $\phi > 5 \times 10^{10} \text{ n/cm}^2$ , the degradation constant

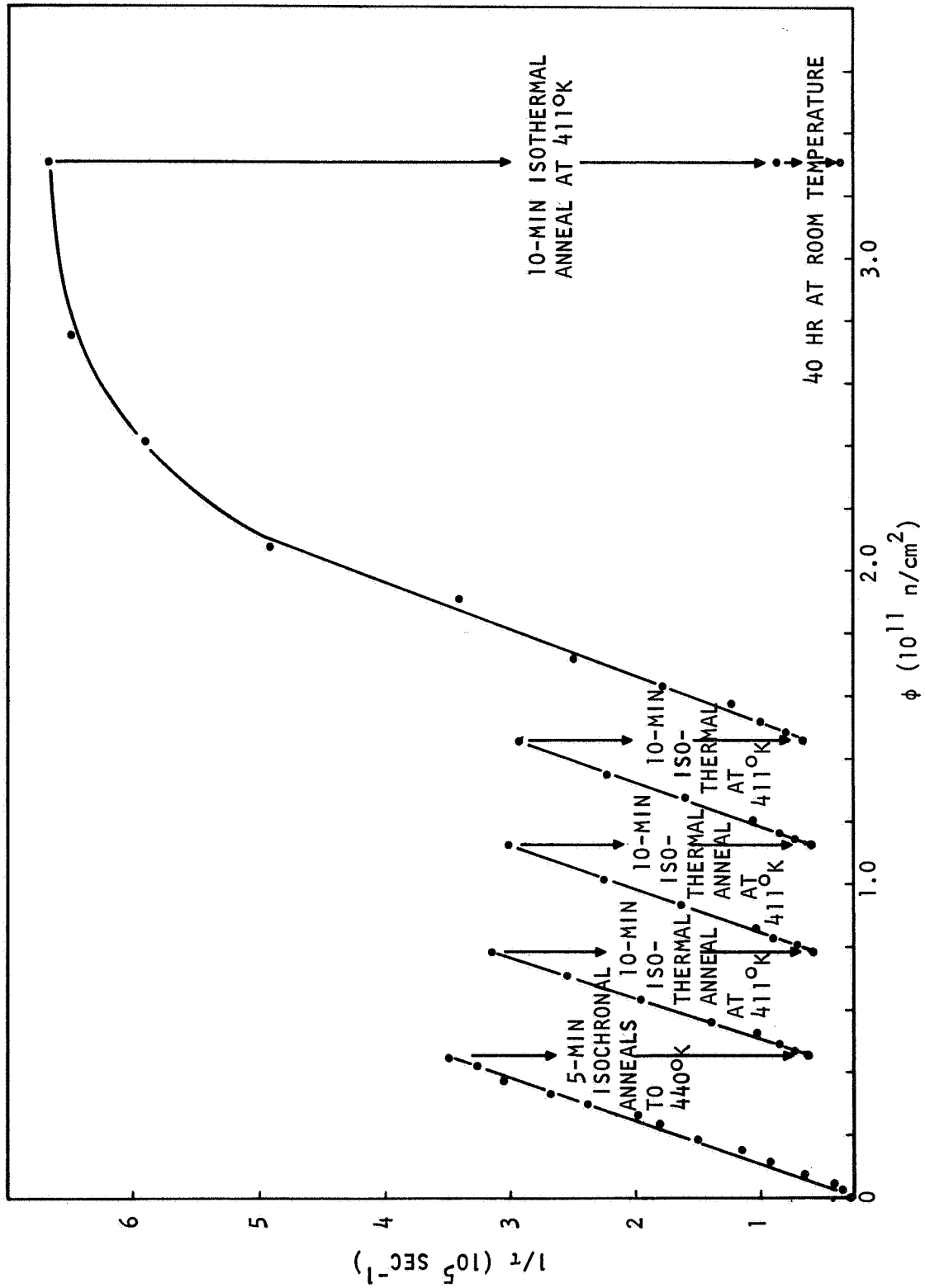


Fig. 15--Inverse lifetime versus neutron fluence irradiated and measured at room temperature

decreased; after the final 10-min anneal at 410°K, the sample recovered only 40 percent of its initial lifetime. This nevertheless corresponds to an anneal of more than 90 percent of the radiation-induced defects after a total fluence of  $\varphi \approx 3.3 \times 10^{11}$  n/cm<sup>2</sup>. Furthermore, after 2 days at room temperature, the sample had apparently further recovered.

Sample b was isochronally annealed for 5-min periods at temperatures between 302°K and 440°K. Figure 16 shows the unannealed fraction versus temperature. The 5-percent annealing at room temperature is due in part to experimental uncertainty. In addition, the room-temperature anneal was actually 10 min long, because we were looking for possible room-temperature isothermal annealing. At 440°K, we observed what appeared to be the beginning of a reverse anneal. This possible reverse anneal was not further investigated at this time.

One isothermal anneal at 411°K was investigated. Figure 17 shows the unannealed fraction of annealable defects as a function of time for both samples a and b for a 411°K isothermal anneal. It is evident that the annealing rate is not significantly different for these two samples.

### 2.3 ACTIVATION ANALYSIS

To date, six silicon samples have been subjected to neutron activation analysis for lithium in an attempt to verify the lithium content estimated by resistivity measurements.

The amount of lithium apparently detected in three of the samples was unreasonably high, so those samples were etched in HF, rinsed in distilled H<sub>2</sub>O again, and remeasured. The lithium detected by the second analysis was about a factor of ten lower than the first.

Unfortunately, the correlation between lithium content as estimated by neutron activation analysis and resistivity measurements is still poor.

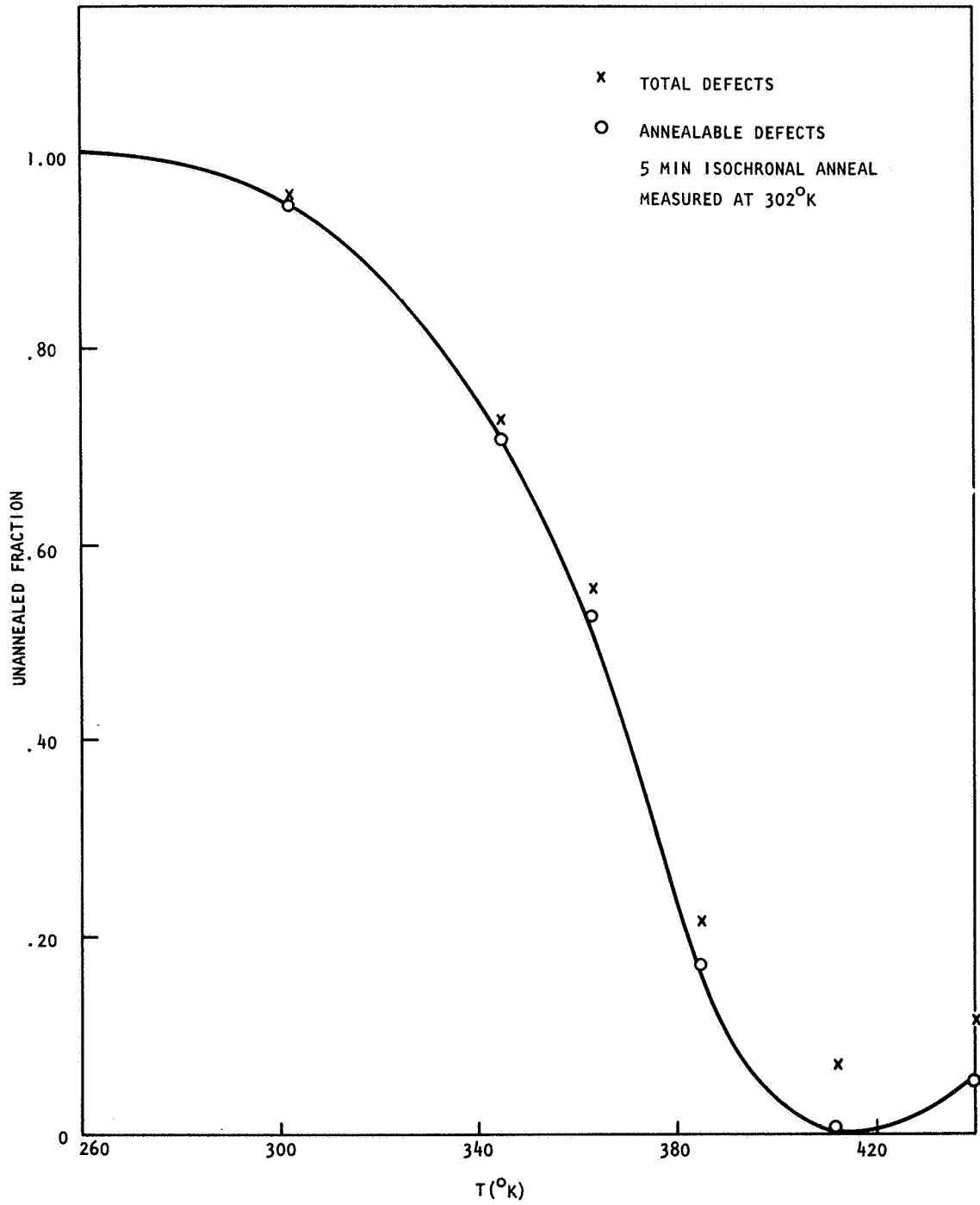


Fig. 16--Unannealed fraction versus isochronal anneal temperature for neutron-irradiated 3.7 ohm-cm sample b

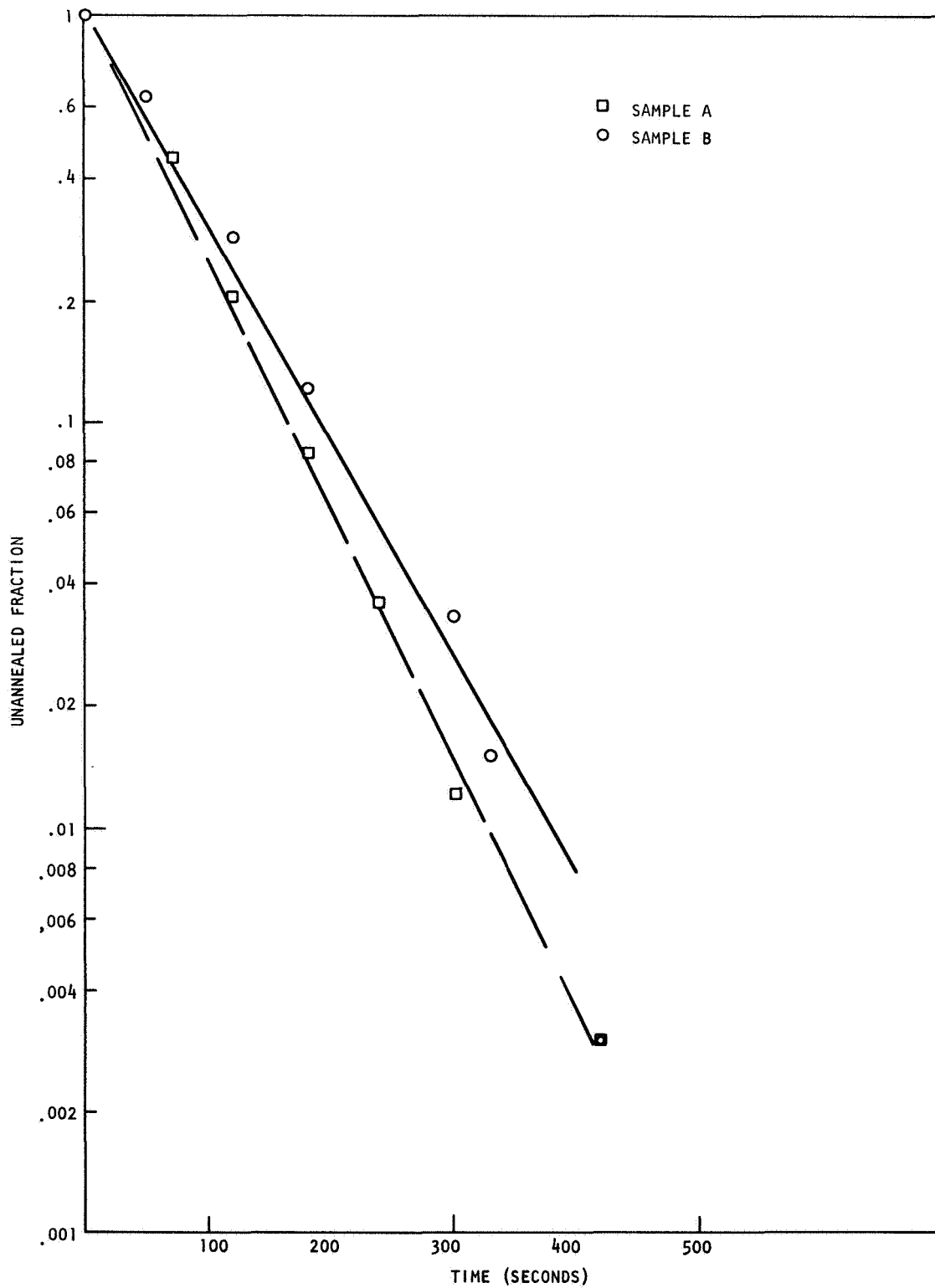


Fig. 17--Unannealed fraction of annealable defects for 411<sup>o</sup>K isothermal anneal versus time. Samples a and b are compared

The actual limit of the measured amount of lithium by activation analysis appears to be about an order of magnitude greater than the interference-free limits of detection, about  $10^{-9}$  g. (9)

The physical size of the samples is limited by the dimensions of the special polyethylene sample containers used in the pneumatic system required to rapidly transfer the sample from the TRIGA reactor to the counting system. The average volume of the samples submitted to date has been  $0.05 \text{ cm}^3$ . The highest lithium concentration has been about  $5 \times 10^{16} \text{ cm}^{-3}$  (0.2 ohm-cm), which corresponds to a total lithium content of about  $3 \times 10^{-8}$  g.

Consequently, activation analysis has indicated only the upper limit of the lithium content of our samples ( $0.2 \text{ ohm-cm} \leq \rho \leq 11 \text{ ohm-cm}$ ). In our most highly diffused sample, activation analyses estimates were three times the lithium estimated by resistivity measurements. While this agreement is disappointing, it would seem to indicate that Li is in the donor  $\text{Li}^+$  or  $\text{LiO}^+$  state and not precipitated for  $n_0 \leq 5 \times 10^{16} \text{ Li/cc}$ , which is consistent with Ferman and Swalin's precipitation rate estimates for low-oxygen-content-silicon. (10) One further test to determine whether or not there is substantial lithium precipitation is possible. We can make a low-resistance sample-- $\rho < 0.1 \text{ ohm-cm}$ ,  $n_0 > 10^{17} \text{ (cm}^{-3}\text{)}$ . By cutting the sample to the shape of a right circular cylinder, we can maximize the sample dimensions subject to the size of the sample vial. This should bring the total lithium content up to about  $10^{-7}$ , which can be accurately measured by neutron activation techniques.

## 2.4 ELECTRON SPIN RESONANCE (ESR)

### 2.4.1 Experimental

The effect of lithium on the B-1 center (oxygen-vacancy) was studied using ESR during the previous contract. (8) In the present program, ESR

will again be used to investigate the effect of lithium on the production and annealing of the divacancy.

Toward this goal, the electron spin resonance apparatus was modified. The microwave plumbing for the superheterodyne ESR spectrometer was assembled as shown in Fig. 18. Microwave power from the LFE 814 stable oscillator is split at the magic tee into the cavity and reference arms of the spectrometer. This bridge arrangement is first nulled using the attenuator and phase shifter in the reference arm; then it is tuned away from null using only the phase shifter, thus producing a bridge sensitive to the dispersion mode. Microwave power is reflected from the reference and sample arms into the detection arm of the bridge.

The ESR signal and the local oscillator signals are fed into a magic tee balanced mixer. This unit takes the difference of the two signals and provides a 60-Mc IF signal which can be amplified electronically by the IF amplifier. This signal is then fed into a PAR 121 phase-sensitive detector, where it is demodulated from the 1-kc audio-frequency-field modulation signal and finally displayed on a strip-chart recorder.

The dewar surrounding the  $TE_{101}$  aluminum cavity was vacuum checked and thermally cycled. A small amount of DPPH was placed in the cavity and the entire spectrometer operation, including noise levels, was checked and found to be operating properly.

The cavity Q, voltage reflection coefficient, and incident microwave power were measured. The amount of microwave power incident on the cavity was calibrated against the crystal at the output of the LFE stable oscillator and the 50-dB precision attenuator. This information is necessary in determining the passage conditions.

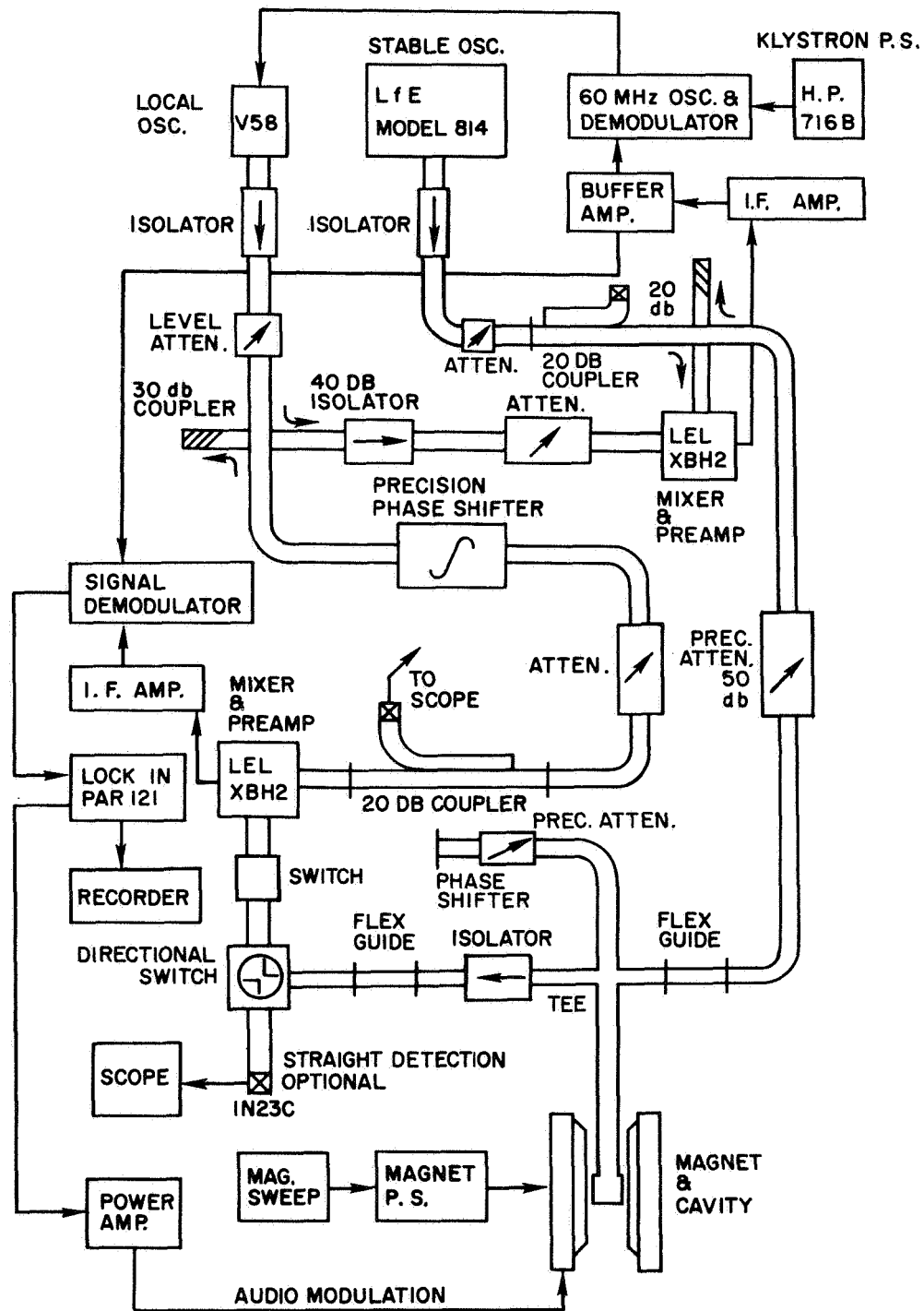


Fig. 18--ESR spectrometer for lithium-doped silicon studies

A small coil was placed in the sample position in the  $TE_{101}$  aluminum cavity to measure the amount of the 1-kc audio-field modulation which actually reaches the sample as a function of temperature. The field was calculated against a 0.4-ohm measuring resistor in series with the audio-field modulation coils. This information is also necessary in determining the sample passage conditions.

#### 2.4.2 Measurements

The divacancy in n-type silicon is paramagnetic only when it is in a single negative charge state. This means that for all of the divacancies to be "seen" by the ESR technique, there must be a sufficient number of electrons in the conduction band to populate all of the centers. This requires an accurate knowledge of the Fermi-level position, which is obtained from sample resistivity measurements.

Four ESR samples have been cut out of a slab of lithium-doped silicon, which has a resistivity of 0.66 ohm-cm as measured by the four-probe technique. The microwave cavity dimensions, applied microwave magnetic field inhomogeneties in the cavity, and the sample-loading tube dimensions dictate a maximum sample size of about 2.3 by 1.2 by 6.4 mm. The four ESR samples were cut to these dimensions.

The resistivity of these small samples must be known as accurately as possible, for the reason given above. Four-probe resistivity measurements of the small samples gave a value 140 percent higher than the true value of 0.66 ohm-cm. Experiments indicated that the small samples were indeed 0.66 ohm-cm, but since the sample dimensions were of the same order as the probe spacing (1 mm), an error was introduced in the four-probe measurements.

Valdes<sup>(11)</sup> used a method of images of the current sources to arrive at six correction factors to be applied to four-probe data when the sample size and probe spacing are of the same order. Using this same technique

in the three cases of interest here--(1) probes perpendicular to a nonconducting boundary, (2) probes parallel to nonconducting boundaries, and (3) probes on top of a thin-slice nonconducting bottom surface--three correction factors were obtained which reduced the error to about 40 percent above the true value of 0.66 ohm-cm. These calculations involved several assumptions, the most important of which is that the above three cases are independent of each other, which is not valid for our small samples. However, the calculations do suggest that the higher measured resistivities of the small samples are due to the small dimensions of the sample and not to some other effect.

To check this postulation experimentally, a phosphorus-doped silicon sample of known resistivity (0.53 ohm-cm) was cut to the same dimensions as the ESR samples, and measured using the four-probe apparatus. It too gave a measured value of about 140 percent higher than the true value (to within the 10 percent repeatability of the four-probe measurements). Thus, a known correction factor can be applied to these four-probe measurements of the small ESR sample to determine the Fermi-level position.

### 3. ANALYSIS AND CONCLUSIONS

In the electron-irradiated samples, fluences beyond which lifetime recovery at 370°K is inhibited have been determined. This inhibition might be attributed to the depletion of lithium, which is capable of annealing damage.

In the neutron-irradiated samples, the degradation constants at 273°K and 302°K were found to be  $(6.4 \pm 0.4) \times 10^{-6}$  cm<sup>2</sup>/n-sec. Isothermal and isochronal annealing behavior indicates activation energies of around 0.68 eV and atomic frequency factors on the order of  $10^7$  sec<sup>-1</sup>, which suggests that the anneal is due to mobile lithium.

#### 4. PLANS FOR THE NEXT REPORTING PERIOD

Plans for the next reporting period include:

1. Continue the electron-irradiation program with an attempt to measure the irradiation temperature dependence of the lifetime degradation constant.
2. Measure the preirradiation and postirradiation preanneal temperature dependence of the lifetime in order to determine the characteristics of the radiation-produced recombination center.
3. Continue the neutron irradiation program with an attempt to measure the postirradiation preanneal temperature dependence of the lifetime.
4. Attempt to measure the irradiation temperature dependence of the lifetime degradation constant for lithium-diffused n-type silicon.
5. Investigate the possible reverse anneal at  $T > 420^{\circ}\text{K}$  after neutron irradiations.
6. Pursue the electron spin resonance measurements of the radiation-produced divacancy.

#### 5. NEW TECHNOLOGY

No new technology is currently being developed or employed in this program.

### REFERENCES

1. Reiss, H., and C. S. Fuller, Journal of Metals, February 1956, p. 276.
2. Naber, J. A., and B. C. Passenheim, "Radiation Effects in Silicon Solar Cells," Gulf General Atomic Report GA-9312, 10 April 1969.
3. Kittel, C., Introduction to Solid State Physics, John Wiley and Sons, New York, 1963.
4. Lax, Melvin, Phys. Rev. 119, 1502 (1960).
5. Naber, J. A., H. Horiye, and E. G. Wikner, "Radiation Effects in Silicon," Gulf General Atomic Report GA-8016, 1967.
6. Stein, H. J., J. Appl. Phys. 37, 3382 (1966).
7. Pell, E. M., J. Appl. Phys. 31, 291 (1960).
8. Naber, J. A., H. Horiye, and V. A. J. van Lint, "Radiation Effects on Silicon," Gulf General Atomic Report GA-8668, 20 August 1968.
9. Lukens, H. R., and V. P. Guinn, Second International Symposium on Nucleonics in Aerospace, Columbus, July 1967.
10. Ferman, J. W., and R. A. Swalin, Proceedings of the Fourth International Conference on Reactivity of Solids, Elsevier, 1961.
11. Valdes, L. B., Proc. IRE 42, 420, 1954.